was larger than the upper layers, it could be said that SL type tilt sensors are suitable for the measurement of inner movements also. Also, comparative movement of the slope throughout the depth could be seen. In Fig. 10(b), measurement of tilt angle on the slope top by SL-3 and SSC-2 tilt sensors are shown. SSC-2 showed small change in negative value along X-direction whereas the tilt angles measured by SL-3 tilt sensor were all positive; SLL-3 showing the largest movement. As in the slope surface (SL-1 and SL-2), here also, SLL-3-X showed the maximum movement. This showed the movement of inner layer being more than the outer layer. As SL tilt sensor could measure the movement of inner as well as outer layers, it could be said that this SL tilt is more practical to use in the field than SSC tilt sensors.

Table 1. Properties of model tests.

Slope type	X	Y	SL-1	SL-2	SL-3
SH slope					
SSC-3	+0.03	-0.13			
SLU-X			+0.15	-0.04	
SLL-X			+0.02	-0.07	
LH slope					
SSC-1	+0.06				
SSC-2	-0.02				
SSC-3					
SLU-X			-0.07	-0.05	+0.09
SLM-X			+0.02	+0.02	+0.09
SLL-X			+0.15	+0.15	+0.23

To observe the nature of change in tilt angle just before failure, tilt angle measured by SL-1 for SH slope (after 70 minutes) and SL-2 and SL-3 in case of LH slopes (after 90 minutes) were divided into few curves as shown in Fig. 11(a) and 11(b), respectively, where the inclination of was changed. In case of SH slope little decrease in trend just before final and sharp increment could be seen for SLU-1-X. Laser displacement values (Fig. 11(a)) also showed the similar pattern. In case of LH slope, small increment in tilt angle just before that final and sharp increment could be seen for SLL-2-X and SLL-3-X and SLU-3-X. The trend of inclination of the curves is similar to those shown by the laser sensors although the amount of inclination was different. This might be due to the difference in the position of the tilt sensors and laser sensors. Here, the trend of change in the inclination before failure was not clear for all the sensors set up. This might be due to small time interval of 5 minutes allowed in between each cut which made it little difficult to measure the trend. With the allowance of longer waiting time, clear and distinct failure trend might be obtained.

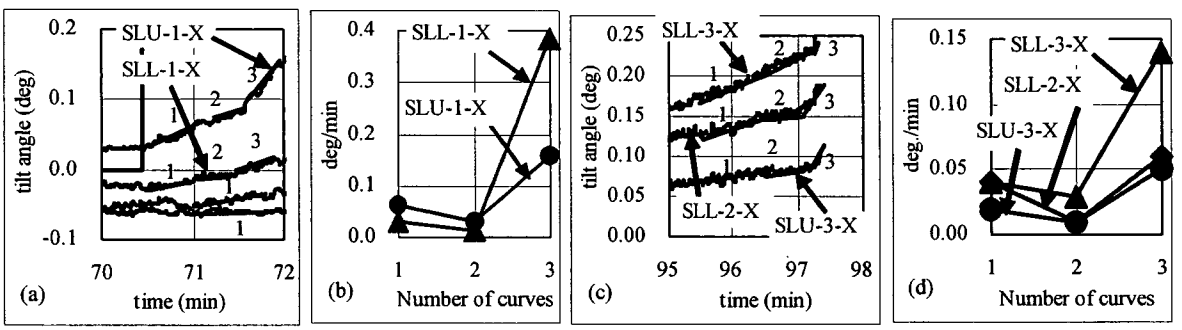

Figure 10. (a) Tilt angle, (b) deg/min curves for SH slope, and (c) tsilt angle and (d) deg/min for LH slope.

5 Conclusions

1. Change in tilt angle with the increment in excavation step could be seen with SSC and SL type tilt sensors.
2. SSC tilt sensor measured only upper layer movement. SL type tilt sensor could measure the tilt angle (movement) of outer and inner layers also. In case of SH, SLU-1 showed larger positive X-direction movement than that by SLL-1. In contrary, SLL-1, SLL-2 and SLL-3, all showed the maximum positive X-direction movement in case of LH slope, thereby showing the larger movement of inner layers of the slope.
3. Tilt angle measured by tilt sensors showed similar trend of increment as those measured by laser sensors. In both the cases, by observing the failure pattern just before the failure, it was observed that the increment in movement with the time decrease for a short time and then it suddenly increased and failed.

Acknowledgement

This work is partially carried out under the Health and Labor Sciences Research Grants of Ministry of Health, Labor and Welfare.

References

Aung, K.K., Rahardjo, H., Leong, E.C., Toll, D.G. 2001. Relationship between porosimetry measurement and soil-water characteristic curve for an unsaturated residual soil. Geotechnical and Geological Engineering. 19, 401-416.

Fredlund, D.G. and Rahardjo, H. 1993. Soil Mechanics for Unsaturated Soils. New York: John Wiley and Sons Inc.

Koseki, J., Matsuo, O. 1997. Liquefaction induced uplift of severe manholes and pipes. Proceedings of Third Asian Young Geotechnical Engineers Conference, Singapore, 549-557.

International Geotechnical Symposium "GEOTECHNICAL ENGINEERING FOR DISASTER PREVENTION & REDUCTION"
July 24-26, 2007, Yuzhno-Sakhalinsk, Russia

Physico-chemical on Mechanism of the Coefficient of Shear Resistance at the Residual State "tan ϕ_r" of Clay

M. Okawara[1], T. Hisatsune[2], T. Mitachi[3]

[1]Faculty of Engineering, Iwate University, Japan
[2]Graduate Student, Iwate University, Japan
[3]Graduate School of Engineering, Hokkaido University, Japan

Abstract

The coefficient of shear resistance at the residual state is a very important parameter in engineering, as usually used for landslide stability analysis. We examined the mechanism of the coefficient of residual state shear resistance "$tan\phi_r$". As a result of AFM measurement of shear surface it became clear that shear surface at the residual state was not a perfect flat, and also by CLSM observation, we found that the contact part of a glass board and a shear surface of clay was only partial contact. It indicates that the area actually touched was smaller than the apparent contact area. The "actual" contact area increased as the normal stress increased. While with FTIR measurement, adsorbed water on shear surface of cohesive soil decreased as the increase in normal stress. In conclusion, the coefficient of residual state shear resistance ($tan\phi_r$) of clay can be thought to be the coefficient originated in the increase in the actual contact area caused by the increase in the normal stress.

Keywords: *coefficient of shear resistance, residual state, clay, chemical and physical property*

1 Introduction

In various shear properties, the coefficient of shear resistance ($tan\phi$), which is an increase rate of the shear stress (τ) to an increase in the normal stress (σ), is an important parameter in engineering study. The states of the shear have peak state, fully softened state and residual state. Residual state is the steady state that the shear strength converges to a steady minimum value after being suffered a large shear deformation. It is known that the slip surface of landslide formed slicken side is in residual state. Mitachi et al. (2003) states clearly that the coefficient of shear resistance at the residual state ($tan\phi_r$) is the same as the coefficient of shear resistance of Hvorslev ($tan\phi_e$) which is thought to be the closest to the true coefficient of shear resistance at present. In other words, "the residual strength IS actual shear strength." Thus, we examined the mechanism of the coefficient of shear resistance at the residual state ($tan\phi_r$). A shear surface at the residual state is flat (Okawara et.al 2003), because particles on a shear surface become oriented after a large shear deformation. So, the shear phenomenon at the residual state can be understood as a friction phenomenon of two flat surfaces in a broad sense. In tribology, the definition of the coefficient of friction μ (F/P) is the ratio of the friction force(F) to the load(P) which is pressing two surfaces vertically. As mentioned above, the coefficient of shear resistance at the residual state ($tan\phi_r$) is the ratio of shear stress τ_r to vertical stress σ ($tan\phi = \tau_r/\sigma$). The coefficient of shear resistance($tan\phi$) is equivalent to the coefficient of friction (μ).The tribological reason for the existence of the coefficient of friction(μ) itself, or the friction force to the load, is that the increase in total actual contact area (Fig.1) is in proportion to the increase in normal stress (Holm,1958;Bowden & Tabor,1964; Greenwood & Williamson 1966). This study is to verify whether the same idea can be applied to the shear of clay. In particular, we focused on 3 points: ①Roughness of Shear Surface, ②Actual Contact Area, ③Spectroscopic Properties of Adsorbed Water.

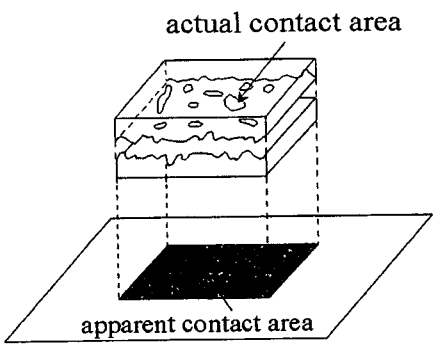

Figure 1. Conceptual diagram of actual contact area.

2 Sample and Experimental Methods

2.1 Sample

The sample used in the experiment was NSF- clay (New Snow Fine-clay). This clay is popular in geotechnical engineering field in Japan. Table 1 shows physical and mineralogical properties of NSF-clay. This clay is composed of a lot of Pyrophyllite and Quartz. Pyrophyllite is clay mineral and Quartz is mainly composed of sand, so NSF-clay is classified into cohesive soil. The specimen used for the observation of a shear surface was a remolded sample. To make this specimen, the deaerated water was added to powdered NSF-clay and remolded by a blender. Then it was put into a cylindrical acrylics cell and deaerated for 30 minutes, and preconsolidated for 7 days with the consolidation pressure of 150kPa.

Table 1. Chemical and Physical properties of NSF-clay.

Soil particle density : ρ_s	2.78g/cm^3
Plasticity index : I_P	41.7
Cation Exchange Capacity:CEC	24.5cmol/kg

2.2 Experimental Method

①Direct shear box test

The shear surface at the residual state made from a long displacement direct box shear test was used for various experiments (Fig.2). Conditions of direct box shear test were: Consolidated constant pressure condition, vertical stress =150kPa; shear displacement =200mm; shear speed =0.5mm/min.

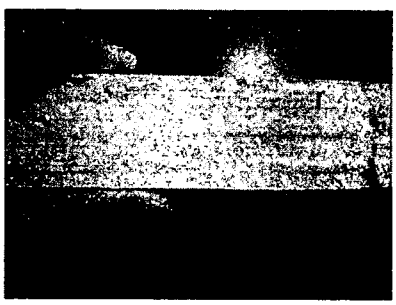

Figure 2. Shear surface at the residual state of NSF-clay.

②AFM (Atomic Force Microscope) Measurement

Asperity measurement and surface analysis of shear surface were done by using AFM (Atomic Force Microscope), namely, Veeco Nano Scope Ⅲ (Fig.3a). The measurement range was 10 μ m×10 μ m. The procedure was as follows. First, soon after the scanning started, 1 skip line was kept, and each parameter was adjusted so that the concave-convex waveform and error waveform of a reciprocating motion became the same. The sample surface was scanned by a tapping method (Fig.3b). Then surface analysis was done from the measured asperity image using the attached software, and the maximum height of the profile (R_{max}), arithmetic mean deviation of the profile (Ra), and increase rate of surface area (RIA) were calculated. Roughness was also quantified by using Ra and RIA. Ra indicates the arithmetic mean deviation of the profile. It is the total area of gray colored in Fig.4. RIA indicates the increase rate of surface area / against flat surface area. As roughness increases, both Ra and RIA also increase.

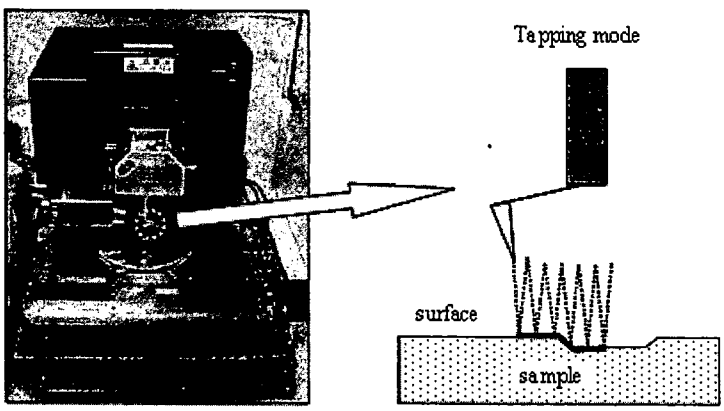

(a) Veeco Nano Scope Ⅲ (b) measurement mode

Figure 3. Atomic Force Microscope.

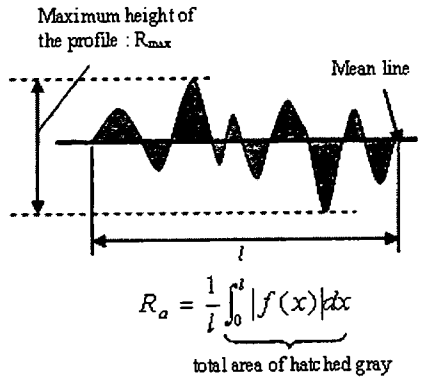

Figure 4. Index of roughness: R_{max}, R_a.

③ CLSM (Confocal Laser Scan Microscope) Observation

The confocal laser scan microscope was used for observing a shear interface. CLSM used for this observation was Bio Rad MRC-1024 (Fig.5a). A confocal laser scan microscope irradiates a sample, detects the light or fluorescence reflected from the sample, and with these data, computer makes the image of the sample. The advantage of this microscope is that it only measures the light from the focal plane that passed through a small hole called a "pinhole" (Fig.5b). By excluding unnecessary light from the upper and lower sides, comparing with the conventional microscopes, its resolution is improved about 1.4 times, so that clear pictures can be expected. Furthermore, even if a sample is thick, we can obtain optical tomograms of the arbitrary depth because a laser can reach deep. An observation was made on a contact plane of a shear surface and a glass. The shear surface formed by the direct box shear test was cut into a size to fit with an observation unit. It was then placed and stuck to a tempered glass which was attached at the lower part of the unit. From the glass side, laser was beamed and the contact part of a glass and a shear surface was observed. The conditions of the observation were, reflection, pinhole diameter:1mm, laser strength:3%, image averaging process:5times.

Moreover, a load unit was used to observe the contact surface when adding normal stress. Figure 6 shows the loading method. The normal stress was added by weights.

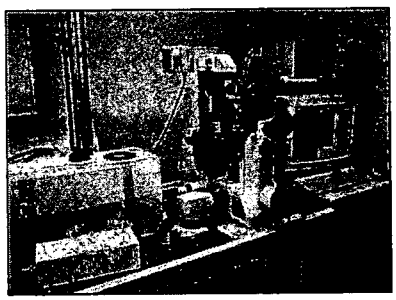

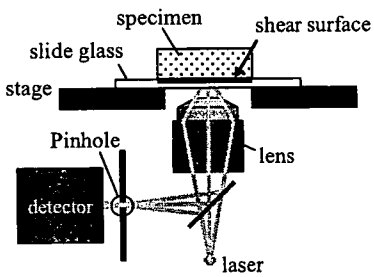

(a) Bio-rad MRC 1024 (b) observation system

Figure 5. Confocal Laser Scan Microscope (CLSM) .

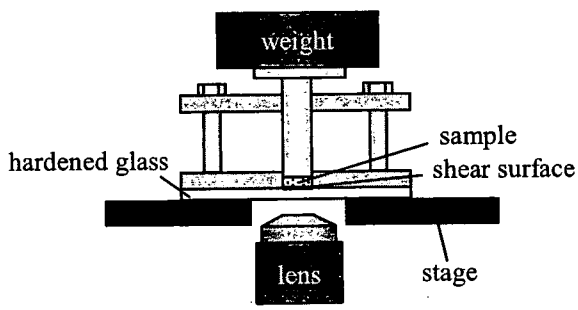

Figure 6. Overview of a pressure unit.

④FTIR (Fourier Transform Infrared Spectrometer) Analysis

In order to clarify the spectroscopic properties of the adsorbed water of a shear surface, it was measured by FTIR (Fourier Transform Infrared Spectrometer). Microscopic-FTIR used for this measurement was JESCO VIR-9500, IR-30 (Fig.7a). The measurement was done by ATR that sticks a prism to a sample surface. Microscopic- FTIR does a great job especially when it comes to a local analysis of a sample surface, and also or a very small quantity of or minute samples. As to this experiment, the diameter was 250 μ m, and measurement depth was 250nm - 2000nm. Background measurement was done first. Subsequently, to perform an infrared spectrum measurement, the shear surface of a sample was touched by a prism of ATR equipment. At this time, the contact pressure of the sample surface and the prism was measured by a small load cell under the sample (Fig.7b). Measurement wavenumber domains :

4000cm^{-1} - 400cm^{-1} of mid-infrared domains, the wavenumber resolution at the time of measurement : 4cm^{-1}, and the number of addition : 87 times.

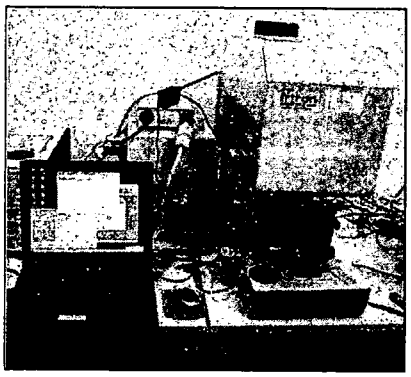

(a) Jasco VIR-9500

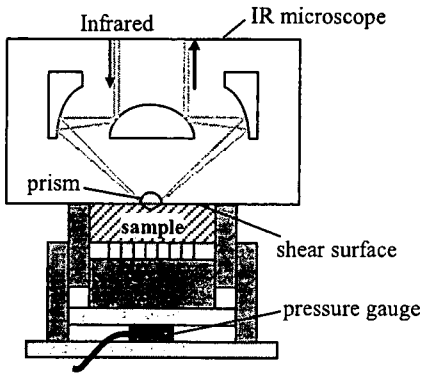

(b) Attenuated Total Reflection-method (ATR), measuring water content of shear surface according to the changes in normal stress

Figure 7. Fourier Transform InfraRed spectroscopy (FTIR).

3 Experimental Results

3.1 Roughness of Shear Surface according to AFM

A concave-convex image of the shear surface at residual state of NSF-clay and a cross-sectional form on ABCD are shown in Fig.8a,b. As shown in these figures, the roughness of the shear surface was confirmed even though the measurement range was very small as to 10 μ m × 10 μ m. The maximum height of the profile of NSF-clay was R_{max}=2085nm, the arithmetic mean deviation was Ra=284nm and increase rate of surface area was RIA=33.67.

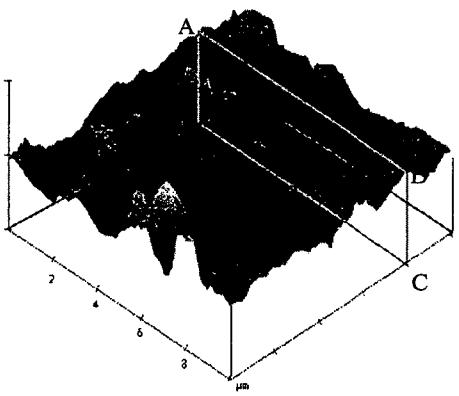

(a) 3D image, Right

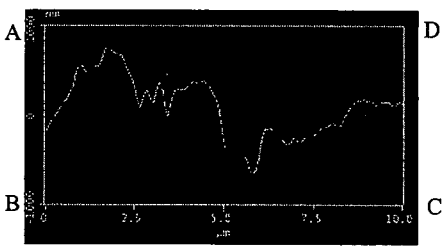

Maximum height of the all profile : R_{max} = 2085nm
Arithmetic mean deviation of the profile : Ra = 284nm
Increase rate of surface area : RIA = 33.67%

(b) Cross sectional form on ABCD and roughness parameters

Figure 8. AFM concave-convex image of the shear surface at residual state of NSF-clay.

3.2 Actual Contact Area according to CLSM

A contact part of a glass board and shear surface of clay was observed from the below by CLSM. Experimentally, we had NSF-clay contact with the glass board. This plane image of the contact part and the cross-sectional image of A-B line are shown in Fig.9. There is a black ellipse at the center of the image (Fig.9a). This part is exactly where the white A-B line is broken in the cross-sectional image (Fig.9b). This means that the black portion is a space. That is, the black portion of the planar image is a non-contact region of particles, and in the case of shear surface, water exists here. The planar image of the contact part of the shear surface and the glass is shown in Fig.10. Different light and dark reflection patterns can be seen on the contact part. If the particles were contacted completely on the shear surface, the image had to be all white. However, the image shows different light and dark patterns, so it is obvious that it was actually contacted only partially. Thus the existence of "the actual contact area" was confirmed. Fig.11 shows when normal stress was increased by a pressure unit. As normal stress was increased gradually (σ v=0kPa, 24.0kPa, 47.7kPa, then to 98.4kPa), the light parts also increased. Here, since the original image of a confocal laser scan microscope is displayed with the gradation from black to white, the neutral color of gray exists. To calculate the rate of area of the contact part, it was difficult to decide whether the gray part belongs to the contact / non-contact part, so the borderline was set to divide all the original images into either "black" or "white" and then total area of "white" was calculated (Table 2, Fig.12). The figure tells us that the area rate of white region was increasing linearly with the increase in normal stress. This indicates that the area that particles of clay and the glass board actually touched, namely "the actual contact area" increased as the normal stress increased.

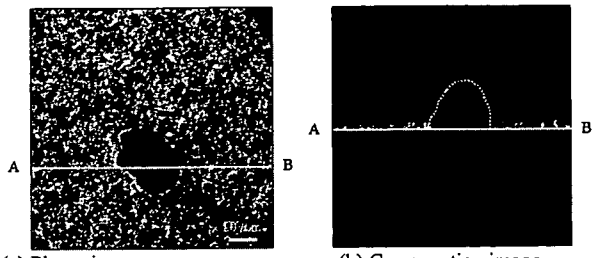

(a) Planar image (b) Cross section image

Figure 9. CLSM images of contact part of NSF-clay with a glass board.

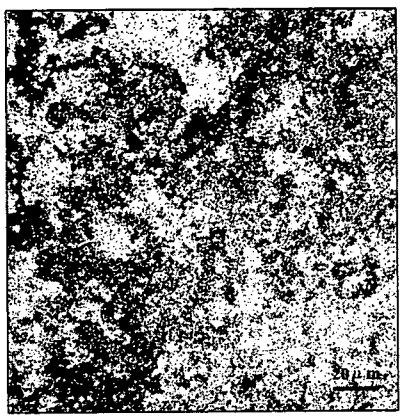

Figure 10. The planar image of the contact part of the shear surface and the glass.

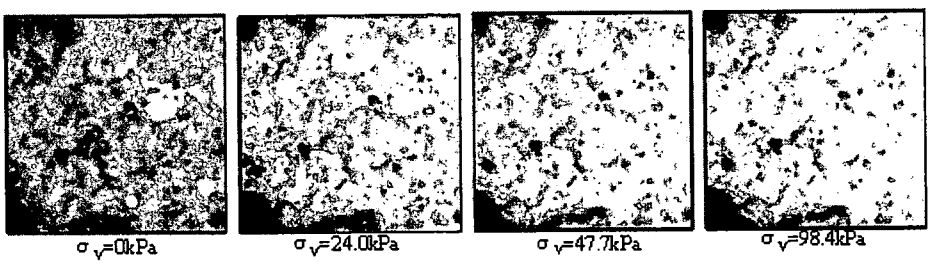

Figure 11. The change in the CLSM image of NSF-clay as the increase in the normal stress (170μm×170μm).

Table 2. Calculated results of white parts.

vertical stress [kPa]	measurement area [μm^2]	total area of white parts [μm^2]	area ration of white parts [%]
0.0	28900	19129	66.19
24.0	28900	21277	73.62
47.7	28900	22803	78.90
98.4	28900	24042	83.19

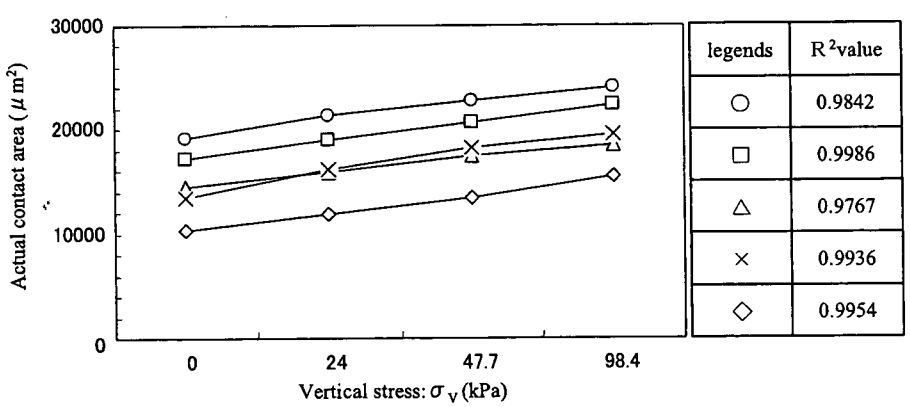

Figure 12. Relation of actual contact area with vertical stress.

3.3 Spectroscopic Properties of Adsorbed Water on Shear Surfaces according to FTIR

The infrared spectrum of adsorbed water on shear surface is shown in Fig.13a. It also shows the spectrum of the bulk water for comparison. From the figure, we can see that the spectrum of the adsorbed water of a shear surface and that of bulk water are similar. The infrared spectrum of NSF-clay, when changing the contact pressure of ATR prism from 10kPa to 40kPa, is shown in Fig.13b. The fine peak group between 3500cm^{-1}-3900cm^{-1} is absorption of steam and the broad peak around 3400cm^{-1} is OH stretching vibration of the adsorbed water near the shear surface of NSF-clay. It is recognized that the absorbance of OH stretching vibration (around 3400cm^{-1}) of an adsorbed water was decreasing with the increase in the contact pressure of ATR prism. It is thought to show the dehydration from the shear surface.

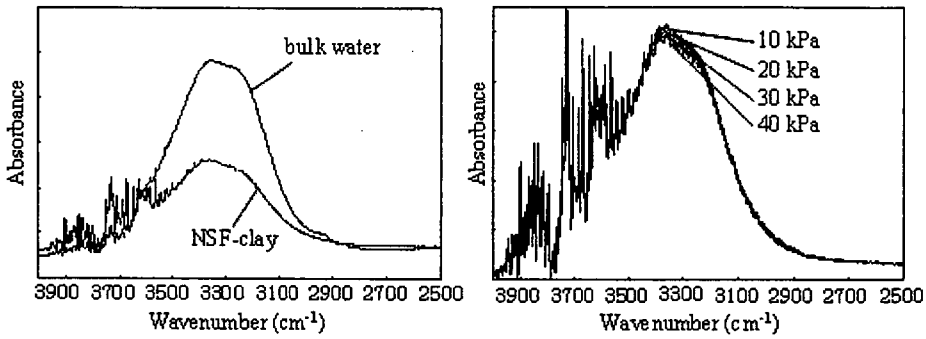

(a) Adsorbed water of shear surface and bulk water (b) NSF-clay when changing the contact pressure of the ATR prism

Figure 13. The infrared spectrum.

4 Discussion

The shear surface which looked flat to the naked eye was actually not completely flat microscopically, and by AFM, it became clear to have concavity and convexity. Moreover, it was realized that the area of contact part becomes larger with the increase in normal stress. In the case of saturated clay, all pores are filled with water, so it is believed that water existing in the non-contact part was observed by CLSM. The infrared spectrum of this water was very similar to that of bulk water, and it was confirmed by FTIR measurement that the water was removed with the increase in normal stress. In conclusion, from these analyses, the coefficient of shear resistance at the residual state can be regarded as "the coefficient resulting from the increase in the actual contact area with the increase in a normal stress". With the plastic body like clay, it is imagined that, even though the surface has unevenness, the shape changes easily and thus contacts completely when it is piled up. However, it is only partial in fact, and this research made it clear that the area of a contact surface becomes larger as the increase in contact pressure. This result was the same as that of the friction mechanism in elastic bodies, such as metal.

5 Conclusion

The following conclusions are obtained.

①A shear surface at the residual state was not a perfect flat, but unevenness existed on it according to the AFM observation. The maximum height of the all profile of NSF-clay was R_{max}=2085nm, the arithmetic mean deviation was Ra=284nm and increase rate of surface area was RIA=33.67%

② The different light and dark reflection patterns were observed on the contact plane of a glass board and shear surface of NSF-clay by CLSM. It means that the contact part was only partial. Thus the existence of "the actual contact area" was confirmed.

③The light parts increased due to the increase in the normal stress by CLSM. This indicates that the actual contact area increased as the normal stress increased.

④The spectrum of the adsorbed water of a shear surface and that of bulk water were similar according to the FTIR.

⑤It is recognized that the absorbance of OH stretching vibration (around 3400cm^{-1}) of adsorbed water was decreasing with the increase in the contact pressure of ATR prism. It is thought to show the dehydration from a shear surface.

The coefficient of residual state shear resistance ($tan\ \phi_r$) of clay can be concluded as the coefficient originated in the increase in the actual contact area caused by the increase in the normal stress.

References

Bowden,F.P. & Tabor,D. 1964. The friction and lubrication of solids, part2, Oxford university press.

Greenwood,J.A.&Willianson,J.B.P.1966.Proceedings.Roy.Soc.,A295,300.

Holm,R..1958. Electric Contacts Handbook, 3rd ed., Springer 247.

Mitachi,T.,Kuda,T.,Okawara,M.,Ishibashi,M.2003.Determination of strength parameters for landslide slope stability analysis by laboratory test and inverse calculation engagement, Jounal of the Japan Landslide Society. Vol.40,No.2, 105-116.

Okawara,M.,Mitachi,T. 2003. Basic research on mechanism of the residual strength of clay, Proceedings of the Third International Symposium on Deformation Characteristics of Geomaterials, IS Lyon, France, 505-510.

MEASUREMENT OF SLOPE MOVEMENT USING TILT SENSOR IN THE SLOPE EXCAVATION FIELD DURING AND JUST BEFORE THE FAILURE

Surendra B. Tamrakar[1], Yasuo Toyosawa[2] & Kazuya Itoh[3]

[1] *National Institute of Occupational Safety and Health (e-mail: tamrakar@s.jniosh.go.jp)*
[2] *National Institute of Occupational Safety and Health (e-mail: toyosawa@s.jniosh.go.jp)*
[3] *National Institute of Occupational Safety and Health (e-mail: k-ito@s.jniosh.go.jp)*

Abstract: Movements of slope surface and slope top just before the failure during the excavation of lower parts of the model slopes were tried to measure using tilt sensors which consists of highly sensitive accelerometers. Accelerometers used here could measure tilt angles along X and Y directions. Depending upon the placement and size of accelerometers set up on the tilt sensor, two types of tilt sensors; Small Compact (SC) and Stand Alone (SA) were designed. Stepwise toe/trench excavations of model slopes were carried out for the model slopes prepared within the laboratory (River sand) and at the field (Narita sand) at regular intervals until failure. Gradual increment in tilt angle along X and Y directions during the excavation and sharp increment just before the failure were observed for both types of tilt sensor, showing the use of these tilt sensors in the real excavating field with high efficiency. In addition to this, with the measurement of X and Y direction tilt angles, prediction of resultant direction of failure movement could also be possible. Deformations measured with laser sensors and linear vertical displacement transducers (LVDTs) in case of laboratory model tests showed similar trend as those by the tilt sensors.

INTRODUCTION

Monitoring of slopes during the excavation works is very important. Excavated slopes become safe only when they are either excavated up to safe slope angle or provided some sorts of protective measures. During the excavation, slopes are at higher risk of failure. In many cases, without any prior signals of failure, instantaneous movement of slope occurs and the workers do not find sufficient time to escape and hence, accidents take place. In Japan, every year around 30 to 40 cases of slope accidents takes place which takes the lives of the workers and damages the properties. More than 50% of such accidents occur while excavating or levelling the lower parts of the slope (toe or trench). To prevent such accidents, it is necessary to monitor the slope movement. With possible early prediction of failure, workers get sufficient time to escape.

In the past and recently, many researches have been presented various methods of measuring the movement of the slope. Japanese Geotechnical Society has given four standard methods for the measurement of the settlement and movement of the slope. Accordingly, in those methods following things are mainly used; a) settlement plate (JGS 1712-2003)(1), b2) displacement wedges (JGS 1711-2003) (2), c) portable extensometers (JGS 1725-2003) (3) and d) water levelling tube which measures the angle (JGS 1721-2003)(4). Among these, the first two methods are applicable to construction works such as embankment above the soft ground. The latter two methods are generally used to measure the movement of the landslide. But all of these methods require some fixed points. In addition, they are time consuming and difficult to set up in the actual real field where slope excavation is going on. In the excavating field where the continuous observation is needed to inform the workers about the current status and to make them escape before the quick failure, the above mentioned methods are not proper.

Many new methods have also been introduced using Optical Fiber Sensors, Non-Prism Total Station, 3-D Laser Scanner, Optical Fiber Extensometer, Fiber Bragg Grating (FBG), Brillouin Optical Time Domain Reflector (B-OTDR), Time Domain Reflectometry (TDR),

Inclinometers, Tiltmeters, etc. These instruments are either used for long-term landslide monitoring or to find the shear plane. To set up of these instruments, bore holes have to be drilled and grouting has to be done. In addition, these are difficult to set up in the real excavating field and require lots of money. Therefore, despite of being reliable, these instruments are not accessible to most of small to medium size contractors. Handling and maintaining the sensitivity are also difficult. Tamrakar et. al (2005) have shown the use of highly sensitive accelerometers as the tilt sensors to measure the slope movement (tilt angle) during the excavation of small scale models within the laboratory. Characteristic increment in tilt angle during the excavation and just before the failure could be observed

In this paper, the above mentioned tilt sensor is tried apply in the real excavating field to see the trend of slope movement of slope during the excavation and just before the failure. Some changes in size of the tilt sensor used by Tamrakar et. al (2005) was done. The one used by Tamrakar et. al (2005) is hereby called SC type whereas the new large size is called SA type. Using SC type tilt sensors along with laser sensors and linear vertical transducers (LVDTs), two laboratory excavation tests were conducted with River sand. Then their measurements were compared. In the real excavating field, model slope of Narita sand was made and movement of slope during excavation was measured with SA and SC type tilt sensors.

TILT SENSORS

Tilt sensor mentioned here consists of highly sensitive accelerometers which are made by anodic bonding of three layers of Silicon (two fixed and one movable) and glass. In principle, capacitance between the movable and fixed electrodes changes when the centre mass of sensor inclines, thereby, changing the gap between the electrodes. By converting the capacitance into voltage and by calibrating tilt angle and voltage later on, one could measure the tilt angle (Takemoto et. al, 2001).

Highly sensitive accelerometers could measure the tilting angle in the range of $\pm 20°$ with the sensitivity of 100mV/deg and have thermal sensitivity of 10mV/°C. Both positive and negative angles along X and Y directions could be measured as shown in Figure 1. Depending upon the requirement of measurement of tilting angle (X and Y directions) and temperature variation, one set of tilt sensor generally comprises of one, two or three accelerometers. Accelerometers are set up on the base plate which is further supported by flat or tubular pipe. Tilt sensor shown in Figures 1 (a) and 1(b) consists of two accelerometers (for X and Y directions) and they are termed as SC (small size compact) type tilt sensor where as the own shown in Figure 1(c) consists of three accelerometers (for X, Y directions and temperature) and they are termed as SA (stand alone) type tilt sensor. SC type tilt sensors are small in size, light to handle and easy to set up (Figures 1(a) and 1(b)). While SA types are bigger in size and need heavy base support (Figure 1(c)). In case of model slope within in the laboratory, tilt sensor shown in Figure 1(a) was used whereas in case of field tests, tilt sensors shown in Figures 1(b) and 1(c) were used.

Direction of movement considered for the tilt sensor was shown in Figure 1. In the models, movements were considered as shown in Figure 2. Here, X represents the movement normal to the slope surface, i.e. inward or outward movements from the slope surface; inward being negative and outward being positive. Similarly, Y represents the movement along the slope surface, i.e. right or left side of the slope. Movement towards right side was considered as positive and that on left side as negative.

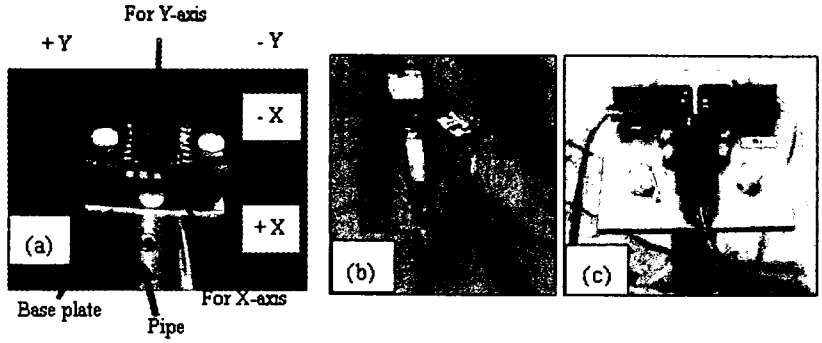

Figure 1. (a) SC type tilt sensor (for laboratory), (b) SC type (for field) and (c) SA type (for field)

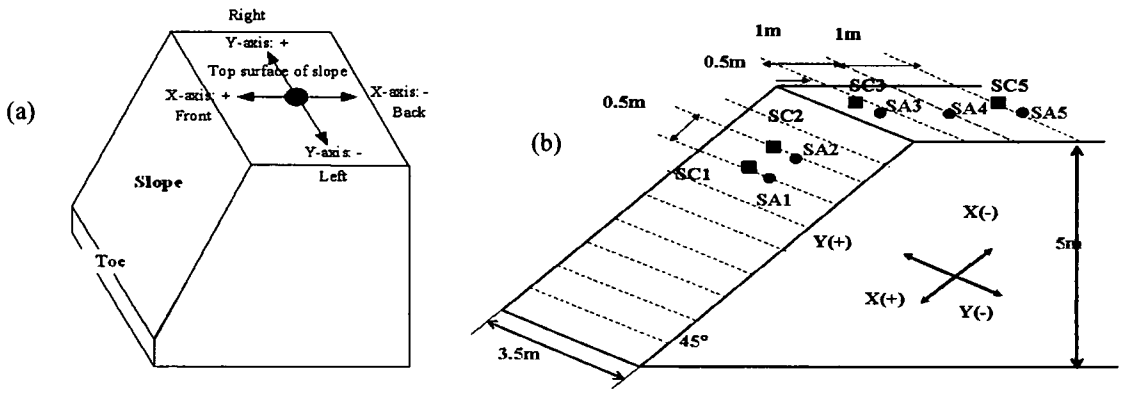

Figure 2. Directions of movement of tilt sensor (a) General outline and (b) Narita sand model

MODEL SLOPES AND TILT SENSOR SET UP

Model slopes were prepared both in the laboratory and in the field to see the applicability of SA and SC type tilt sensors during excavation.

Laboratory test

Small size full scale test was carried out in the laboratory with Frame work (Tamrakar et. al, 2005) made from wooden planks supported externally by the iron bars/beams. The whole frame work could be divided into two sections; lower (1.35m x 2.7m x 1.3m) and upper (1.35m x 1.2m x 0.88m) which facilitate to make different types of slopes with different conditions. River sand was used as the test material. Properties of River sand was shown in Table 1. River sand was poured within the test box consisting of both upper and lower frame. Medium dense test model was tried to obtain by compacting and trimming the sand manually. Due to the compaction, slopes could withstand by itself even after the trimming them into required slope angle.

Two types of slope models were prepared as shown in Figures 3. In case of two-step slope model, lower section was only used, keeping the upper section as load surcharge behind and above the slope top. Here, slope length and height were shorter. One-step slope model was prepared using both upper and lower sections. Hence slope height and length were longer. In total, four slope models were prepared. Slope-II-1 and Slope-V-1 were two-step, short slopes with 60 and 70 degree slope angle, respectively, whereas Slope-II-3 and Slope-V-2 were one-step, long slopes with 50 and 70 degree slope angle, respectively. Slope height for two-step is 1m whereas for one-step is 1.2m. Unit weight and water content for each of these slopes are shown in Table 2. Due to medium dense compaction and side support by the wooden

frames, slopes could withstand by themselves even after the trimming them into required slope angle without failure.

Table 1. Properties of River sand and Narita sand

	River Sand	Narita Sand
Unit weight of soil solid (kN/m^3)	2.76	26.12
2~0.075x10^{-3}m (%)	8.8	
0.075x10^{-3}~2x10^{-3}m (%)	89.1	77.5
0.005x10^{-3}~0.075x10^{-3}m (%)		12.7
<0.075x10^{-3}m (%)	2.10	
<0.005x10^{-3}m (%)		9.8
Avg. particle size, D_{50} (x10^{-3}m)		0.19
Soil classification	SP-G	SF
Sand replacement (unit weight) (kN/m3)		17.09
Sand replacement (water content) (w%)		27.45
Core cutter (unit weight) (kN/m3)		16.16
Core cutter (water content) (w%)		28.75

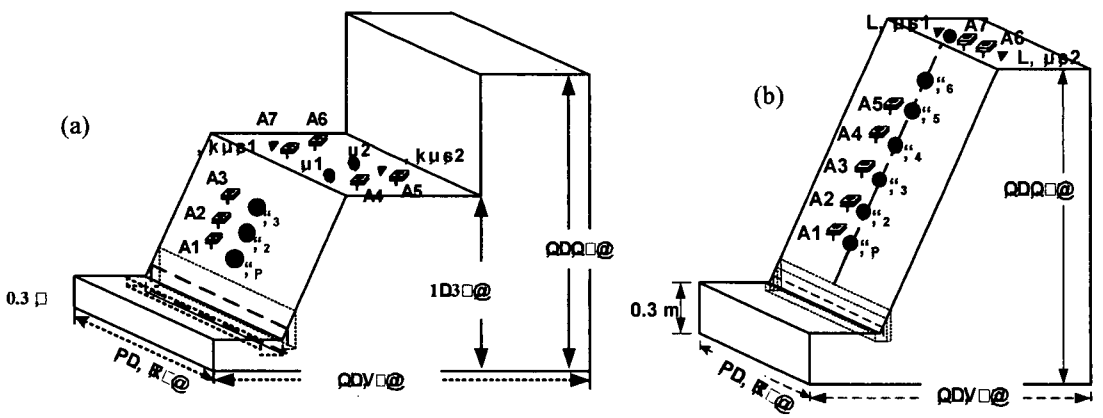

Figure 3. Model slope in the laboratory – (a) Two-steps short slope and (b) One-step long slope

Table 2. Test conditions of laboratory slopes

Test name	Avg. w	Avg. γ_d	Slope angle	Type of the slope	Failure	Failure
	%	g/cm^3	degrees		Steps	Time(minute)
Slope-II-1	8.54	1.38~1.41	60	Two-step, Short	2	6.0
Slope-II-3	8.54	1.38~1.41	50	One-step, Long	2	6.75
Slope-V-1	6.6-7.4	1.45-1.50	70	Two-step, Short	21	192
Slope-V-2	6.6-7.4	1.45-1.50	70	One-Step, Long	7	46.8

SC type tilt sensors were set up on the slope surface and slope top; three (A1, A2 and A3) on the slope surface and four (A4, A5, A6 and A7) on the slope top. Vertical deformation of the slope surface and slope top were also measured using laser sensors and linear vertical displacement transducers (LVDTs). Targets were set up perpendicularly both on the slope surface and slope top. Laser sensors set up on the slope surface is represented by S1, S2, S3 and so on; S1 being closer to toe of the slope. Vertical deformation of the slope top measured by

laser sensors was represented by V1, V2; V1 being close to the crest. Similarly, vertical deformation with LVDTs was represented by LVDT1, LVDT2; LVDT1 being close to slope crest. Tilt sensors and deformation measuring laser sensors and LVDTs were placed almost in the same position. Sequences/locations of tilt sensors and deformation measuring target points are shown in the Figures 3.

Excavation was done manually with scoop from the toe of the slope. In case of Slope-II-1 and Slope-II-3, excavation was done at toe (without trench excavation) in steps as shown in Figure 4. For Slope-V-1 and Slope-V-2, both toe and trench excavations were carried out in steps. In all the cases, excavations were continued until the slope failure was occurred. In case of Slope-II-1 and 3, the first trench was 15cm in depth and 15cm in width. After that, each toe excavation was 5cm in width. In contrary, for Slope-V-1 and 2, depth and width for both trench and toe excavations were around 5cm and 10cm, respectively. Some variations in the depth and width of cut of excavation were there. Time interval between each step of excavation was around 5 minutes so that movement of slopes as well as the slope top could be observed. For Slope-V-1, total numbers of excavation steps were 21 whereas for Slope-II-1, slope failed all of sudden after 2nd cut. Total number of cuts and total elapsed time for failure were also shown in Table 2.

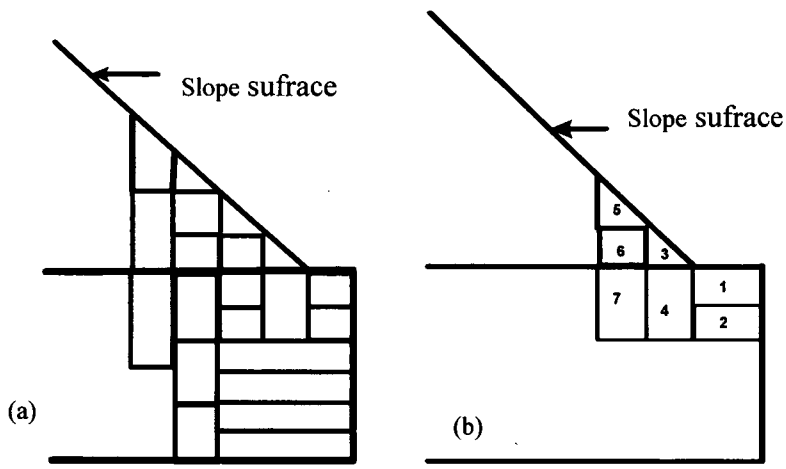

Figure 4. Steps of Excavation (a) slope-V-1 and (b) Slope-V-2 in the laboratory

Field test

Model slope was prepared in the field from Narita sand, collected from the Toke Construction site, Chiba, Japan. Model slope was prepared by compacting the soil with small size bull dozer and trimming the slope surface by back hoe. The height, width and slope angle of each model slope were 5m, 3.5m and 45°, respectively. Outline of the model slope is shown in Figure 2(b). At 2.5m and 5m heights, density and water content of the model slopes were measured by Sand replacement method and Core cutter. Properties of Narita sand along with average unit weight and water content for each model slopes are shown in Table 1. Four SC (SC1, SC2, SC3, and SC5) and five SA (SA1, SA2, SA3, SA4 and SA5) type tilt sensors were set up both on the on the slope surface and slope top. Slope surface was divided into 10 equal widths and excavation was started from the toe of the slope, vertically downward using a back hoe. Height and width of each cut were therefore change by 0.5m. About 5 minutes waiting time was allowed between each cut. Toe excavation was continued until complete failure of slope was occurred. Directions of movement of tilt sensor on the model slope were shown in Figure 2. In total 6 cuts were made. Partial failure was seen after 5th cut. But the final failure

was observed after 6th cut at around 51 minutes of elapsed time. During the excavation, tensile crack was appeared on the slope top.

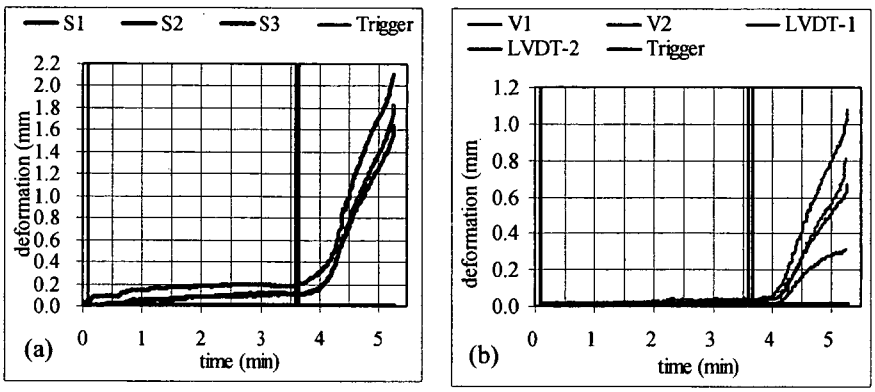

Figure 5. Deformation for Slope-II-1 (a) Slope surface and (b) Slope top

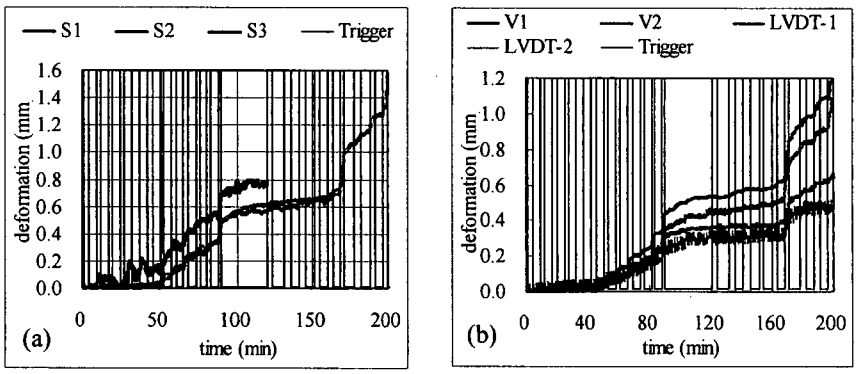

Figure 6. Deformation for Slope-V-1 (a) Slope surface and (b) Slope top

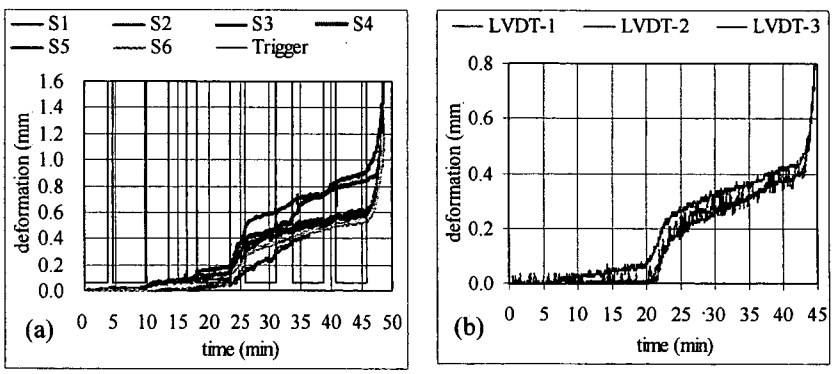

Figure 7. Deformation for Slope-V-2 (a) Slope surface and (b) Slope top

RESULTS AND DISCUSSIONS

Laboratory test

In Figures 5, 6 and 7, deformations measured on the slope surface and top of the slope were shown. Bold vertical lines in the figures show the finishing line of excavation. For Slope-II-1 and Slope-II-3 (not shown in the figure), failure took place around 5.25 and 6.75 minutes,

respectively. Similarly, for Slope-V-1 and Slope-V-2, failure took place around 192 and 46.8 minutes, respectively. Comparing the total time taken, it could be observed that the first two slopes failed very faster than the later ones. The reason for it is that the first two slopes were lightly compacted and had higher water content than those of later slopes. Comparing the total time taken for Slope-V-1 and Slope-V-2, it was observed that the slope having longer slope length failed faster. Hence Slope-V-2 failed faster than Slope-V-1.

In all the test cases, with the increase in excavation steps, gradual increment in deformations of slope surfaces and slopes tops could be seen. Trend of deformation measured on the slope surface and slope top were also same. Increment in deformation became maximum and sharp just before the failure in all the cases. In all the test cases, laser sensors and LVDTs placed nearer to the excavation site and slope crest, respectively, showed the maximum value just before the failure. This shows the most possible places for the measurement of deformation during the excavation so that the advance prediction of failure could be done. Also, from the test results, it could be said that the deformation measured on the slope were comparatively larger than vertical deformations measured on the slope top. Therefore it is suggested to measure the movement of the slope surface.

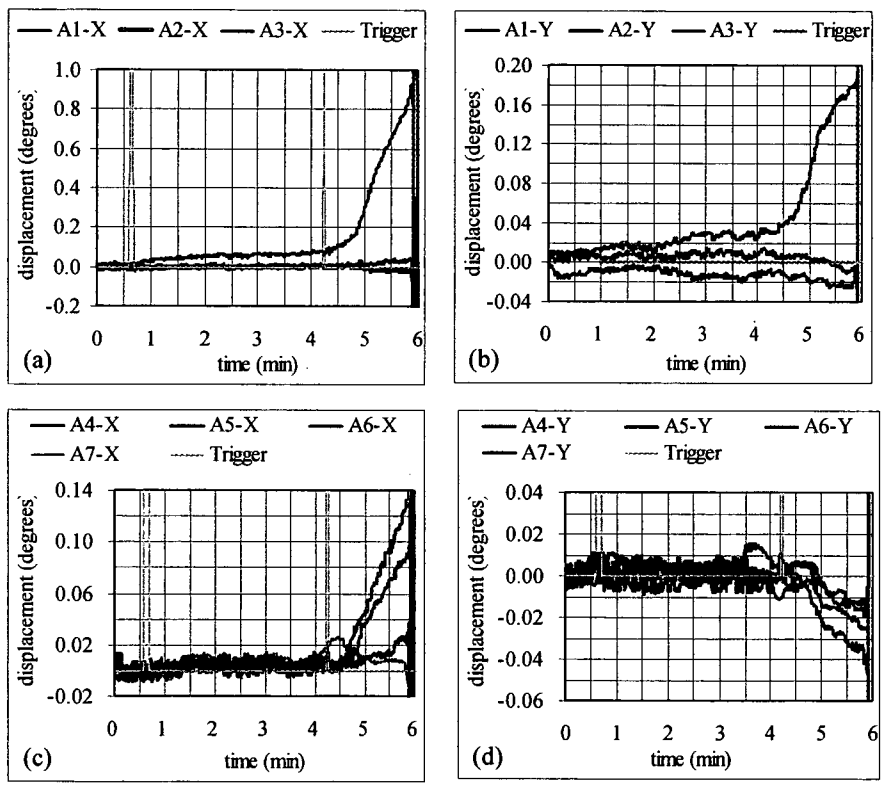

Figure 8. Tilt angle measurement (SC type sensor) for Slope-II-1

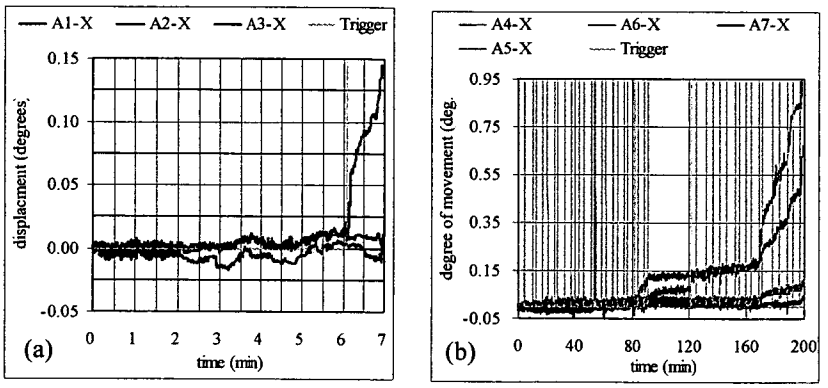

Figure 9. Tilt angle measurement (SC type sensor) (a) for Slope-II-3 and (b) for Slope-V-1

Measurement of tilt sensors placed on the slope surface (A1, A2 and A3) and slope top (A4, A5, A6 and A7) for each model tests could measure the tilt angle. In Figure 8, X and Y directions movement for Slope-II-1 for the slope surface and slope top were shown. Similarly, movement along X direction for Slope-II-3 and Slope-V-1 were shown in Figure 9. At the beginning where small excavations were only made, clear increment in tilt angles was not seen. But after certain elapsed time, gradual increment in tilt angle was seen, which sharply increases just before the failure. Trend of sharp increment is similar to those obtained for deformation measurement on the slope surface and slope top. This shows the applicability of possible measurement of slope failure pattern so that the prediction of failure could be done in advance.

For loosely compacted slopes (Slope-II-1 and Slope-II-3), sharp increment and change in tilt angle were seen after 2nd cut where as for Slope-V-1 and Slope-V-2, slopes were failed after 21st and 7th cuts. As in the deformation of slopes, here also, tilt sensor placed near the excavation site showed the maximum values. This showed the importance of setting up positions for the tilt sensors on the slope surface and slope top. But the position of setting up the tilt sensor is important. In case of Slope-II-1 and 3, as the compaction was loose, even with two cuts, failure took place whereas in Slope-V-1 and 2, excavation reached up to the position of A1 before failure.

Comparing the tilt angles measured on the slope top for small slopes (Slope-II-1 (Figure 8(c) Slope-V-1(Figure 9(b)) along X and Y directions, similar trend of movement were seen. These also show the possibility of measurement of tilt angle just before the failure. Tilt sensors placed far away from the slope crest showed the maximum movement in both the cases. This might be due to failure plane (tensile crack) passing between the first row (A4, A6) and second row (A5, A7) tilt sensors. As tilt angle along X and Y direction could be measured, it is possible to predict the direction of movement of slope during failure.

Field test

Tilt angle measured with SC and SA type tilt sensors along the slope surface (SC1, SC2, and SA1, SA2) and slope top (SC3, SC4 and SA3, SA4, SA5) was shown in Figures 10 and 11. In the figures mentioned here, solid vertical lines represent the number of cut and dashed lines in between the solid lines represent the occurrence of partial failure whereas the dashed line at the end represents final failure. Although it is difficult to see the amount of movement for the first few cuts, increment in the slope movement with the progress of cut could be seen in all the sensors. Sudden increment in the tilt angle was seen after 5th and 6th cuts in case of Narita sand (H). Partial failure was stopped after 44 minutes and then final failure of whole slope took place around 51 minutes. During the failure, whole slope moved towards the left side of the slope face. Direction of slope failure could also be determined by observing the movement of tilt sensors along X and Y directions. By comparing the tilt angle of SC tilt sensors set up on the slope surface in case of Narita sand (H), SC1 and SC2 tile sensors both showed negative

movement along X and Y directions, showing the movement of slope surface inward and toward the left side of the slope face whereas SC3 and SC5 tilt sensors showed the positive movement along Y direction, showing the movement of slope top outward and towards the left side of the slope face. This shows the failure of slope for Narita sand (H) towards the left side of sloe face by overturning of upper section of slope (slope crest). Similar movements were seen for SA tilt sensor also. Changes in the tilt angle for each SC and SA tilt sensors along X-direction at particular elapsed time were shown in Table 3. Both SC and SA tilt sensors showed almost same value. This shows the applicability of both types of tilt sensors in the field with equal efficiency.

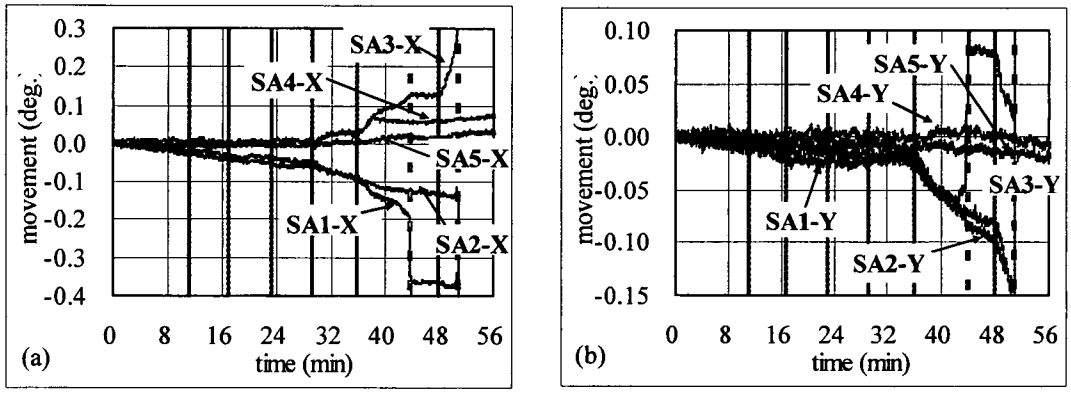

Figure 10. SC type tilt sensor measurement for Narita sand model (a) X and (b) Y directions

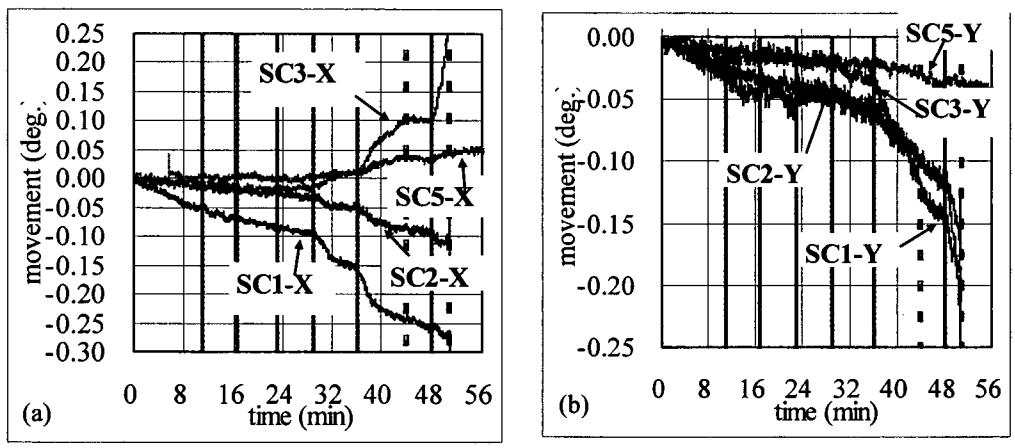

Figure 11. SA type tilt sensor measurement for Narita sand model (a) X and (b) Y directions

Table 3. Tilt angles measured along X-axis

Narita sand (H) (around 51 min. elapsed time)					
tilt-angle	1	2	3	4	5
SC	-0.275	-0.11	0.25	-	0.025
SA	-0.300	-0.15	0.25	0.06	0.025

CONCLUSIONS

1. Both SC and SA type tilt sensors showed gradual response with the time and step of excavation. Sharp and steep changes in the tilt angle both on the slope surface and slope top just before the failure was possible to measure. Hence both tilt sensors could be used to predict the slope failure in advance.

2. With SC and SA type tilt sensors, it is possible to measure the tilt angle along both X and Y directions. This could be used for the prediction of possible direction of resultant failure movement of slope during failure.
3. In case of laboratory test, the trend of movement of SC tilt sensors is similar to the movements of slope surface and slope top measured by laser sensors and LVDTs. Measurement of steep and sharp changes in the movement and deformation just before the failure shows the possible prediction of failure in advance.
4. Laser sensor and LVDTs which were set up closer to the excavation site and slope crest, respectively in the laboratory test, showed the sharp and maximum deformation. This shows the possible position for the set up of instrument for the measurement.
5. In case of Narita sand, in the field, both SC and SA tilt sensors showed almost same pattern and same amount of tilt angle. This suggests that both SC and SA tilt sensors could be used with equal efficiency.

Acknowledgements: This work is partially carried out under the Health and Labour Sciences Research Grants of Ministry of Health, Labour and Welfare.

REFERENCES

TAKEMOTO, M,. SATOU, A., MATSUYAMA, H., OGATA, K., KUNIMI, T., ITOH, S. & NEZU, M. 2001. Development of new In-place inclinometer in bore using accelerate sensor. *36th Annual meeting of Japanese Geotechnical Society*, 179-180.

TAMRAKAR, S.B., TOYOSAWA, Y. AND KAZUYA, I. 2005. Measurement of slope movement during the slope excavation of small size full scale model. *International Symposium on Landslide Hazard in Orogenic Zone from the Himalaya to Island Arc in Asia*, 265-274.

JGS 1712-2003. Japanese Standards for geotechnical and Geo-environmental Investigation Methods- Standards and Explanations- Methods for measuring settlement of ground surface using settlement plate, *Japanese Geotechnical Society*, Japan, 609-610.

JGS 1711-2003. Japanese Standards for geotechnical and Geo-environmental Investigation Methods- Standards and Explanations- Methods for measuring displacement of ground surface using stakes, *Japanese Geotechnical Society*, Japan, 617-618.

JGS 1725-2003. Japanese Standards for geotechnical and Geo-environmental Investigation Methods- Standards and Explanations- Methods for measuring displacement of ground surface using extensometer, *Japanese Geotechnical Society*, Japan, 619-620.

JGS 1721-2003. Japanese Standards for geotechnical and Geo-environmental Investigation Methods- Standards and Explanations- Methods for measuring tilt of ground surface using tiltmeter, *Japanese Geotechnical Society*, Japan, 628-630.

Development of new tensile strength measuring apparatus for soils with suction measurement

S.B. Tamrakar, T. Mitachi, Y. Toyoswa & I. Kazuya
Construction Safety Group, National Institute of Occupational Safety and Health, Tokyo, Japan-204-0024
tamrakar@s.jniosh.go.jp

ABSTRACT: New type of tensile strength measuring apparatus was developed which could measure the tensile strength and suction of the soil specimens (both saturated and compacted) from the start to the end of the test. Three saturated specimens of NSF clay consolidated under 50, 108 and 197 kPa were used. Increment in tensile strength and suction with the increase in consolidation pressure was observed. Suction was measured at two positions of the specimen; (1) at the bottom and (2) at the mid height and it was observed that both of these suction showed similar trend in increment with closer values. In addition, suction was increased to its maximum value when tensile stress reached to its peak value. Tests were conducted by varying the tensile pulling rate from 0.001 to 1.0 mm/min and it was observed that both tensile strength and suction values increased with the increase in the tensile pulling rate.

1. INTRODUCTION

Tensile strength of soils is usually not taken into account when solving typical geotechnical problems. But the development of tensile crack which leads to the failure of slopes, earth dams, embankments, pavements and ice lens development process during freezing of soil is related to tensile strength. Tensile cracking usually occurs when induced tensile stress and strain exceed the tensile strength and allowable tensile strain of the soil, respectively. Hence the precise measurement of tensile strength is necessary. Different researchers have tried to measure the tensile strength of soils; directly and indirectly. Among direct methods, those developed by Yao et al. (2002), Ono et al. (2003), Nahlwi et al. (2004) and Tamrakar et al. (2005) are suitable for measuring the tensile strength from fewer kilopascals to higher values of saturated and unsaturated (compacted) soils.

Tensile strength of soil varies from fewer kilopascals to higher values depending upon the saturation condition of the soils; highly saturated soils showing smaller tensile strength than partially saturated soils. This variation in tensile strength with saturation condition is related to suction values of soil. To evaluate the relationship between the tensile strength and suction, measurement of suction during the tensile pulling is necessary. But the apparatuses developed earlier by present authors could not measure the suction directly. In those cases, suction was measured indirectly using the relationship of water content and soil-retention curve which gives the approximate suction of the specimen only. But the measurement of suction directly and from the start of tensile pulling test to end of tensile failure is important so that the behavior of suction with the tensile stress could be seen. Also, variation in tensile strength and suction with the change in tensile pulling rate is necessary to study. In this paper, a new type of tensile strength measuring apparatus was developed which could measure tensile strength of soil (saturated and compacted) along with the suction from the start to the end of the test. Suction is tried to measure at two positions of the specimen; (i) at the bottom and (ii) at the mid height. Also, change in tensile strength and suction with the change in tensile pulling rate (0.001 to 1.0 mm/min) was measured.

2. NEW TENSILE PULLING APPARATUS

A new type of tensile pulling apparatus is developed here in reference to Tamrakar et al. (2005). As shown in

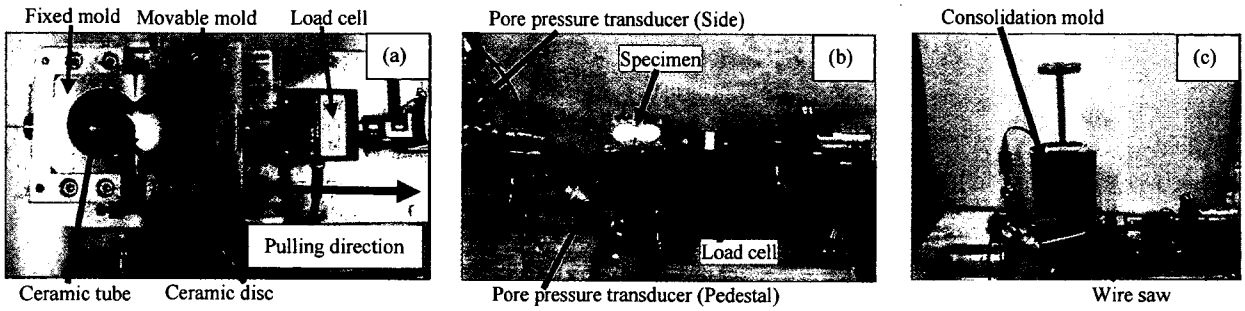

Fig. 1 (a) Ceramic tube, ceramic disc and tensile molds, (b) pore pressure transducers and (c) consolidation mold

Figures 1a,b, it consists of fixed and movable molds which look alike. Both the molds are attached to their base plates one of which is fixed and another one is movable toward the pulling direction as it is placed on a single linear bearing. During the specimen preparation, both the molds are attached to each other by two horizontal screws which are thereafter, unscrewed before the start of tensile pulling. Tensile crack is appeared at the middle portion of the specimen (constricted portion where two molds are attached). The width and depth of this middle portion are 3 cm and 5 cm, respectively. The load cell placed between the movable box and motor axis measures the tensile load. Tensile load measured is divided by the area of the middle portion where tensile crack appears, to calculate the tensile strength. Tensile pulling rate of this new apparatus can be varied from 0.001 to 1.0 mm/min.

As shown in Figure 1a, to measure the suction, ceramic disc and ceramic tube were placed at the bottom and mid height of the fixed mold, respectively. The air entry value (AEV) of these ceramics is 240 kPa. Suction measured by ceramic disc and ceramic tube is represented hereby as Pedestal and Side suction, respectively. Ceramic disc is placed below the specimen before or after the specimen preparation depending upon the type of the specimen. In case of saturated specimen, it is placed from the beginning before inserting the specimen into the mold. In case of compacted (unsaturated) specimen, at first ordinary disc (without ceramic disc) is placed at the bottom during the compaction. Once the compacted specimen is ready, then it is replaced by the ceramic disc. In contrary to ceramic disc, ceramic tube is inserted from the side of the fixed mold (Fig. 1a) only after the specimen is prepared within the tensile mold. Ceramic disc and ceramic tube are connected to differential pore pressure transducers placed outside as shown in Figure 1b, which measure the pore water pressure. Suction is given by the difference of pore air pressure (here, it is atmospheric pressure = 0 kPa) and pore water pressure. Therefore, suction becomes positive if measured pore water pressure is negative.

3. SPECIMEN PREPARATION AND TEST SET UP

NSF clay is commercially available artificial clay. It consists of mainly pyrophyllite and quartz minerals. In this paper, only saturated test cases are explained. At first, slurry of NSF clay was prepared by thoroughly mixing powder of NSF clay to distilled water. Amount of distilled water mixed was about 1.5 times the liquid limit of NSF clay. Prepared slurry was then poured into the consolidation mold placed within the big cell where vacuum was applied to remove the entrapped air bubble. Once the air bubble was removed, then consolidation mold was taken out of the big cell and consolidation was started in steps. Specimens were prepared under three consolidation pressures; 50, 108 and 197 kPa. After the consolidation, with the help of guiders, consolidated speciemen was inserted into the tenilse mold as shown in Figure 1c. Prior to the insertion, all the connecting lines between the ceramic disc, ceramic tube, pore water pressure transducers, valves, etc., were thoroughly flushed and de-aired with distilled and de-aired water. Just before inserting consolidated specimen within the tensile mold, thin film of water above the ceramic disc was lightly wiped off by the wet cloth. Change in pore water pressure could be seen when inserting specimen base touches the ceramic disc. Insertion was then stopped and upper surface of the specimen was trimmed by wire saw.